Cell Biol Toxicol (2021) 37:51–64
https://doi.org/10.1007/s10565-020-09530-8

ORIGINAL ARTICLE

Human umbilical cord blood–derived MSCs exosome attenuate myocardial injury by inhibiting ferroptosis in acute myocardial infarction mice

Yufang Song · Baocai Wang · Xiliang Zhu · Junlong Hu · Junjie Sun · Jizhong Xuan · Zhenwei Ge

Received: 25 December 2019 / Accepted: 28 April 2020 / Published online: 13 June 2020

Abstract The exosome of MSCs derived from human umbilical cord blood (HUCB-MSC) has been reported to have cardioprotective effects on mouse models of acute myocardial infarction (AMI) and cardiomyocyte hypoxia injury, but the exact mechanisms involved require further investigation. This paper aimed to study the role of HUCB-MSC-exosomes in inhibiting ferroptosis to attenuate myocardial injury. Compared with sham or normoxia groups, RT-PCR and western blotting showed that divalent metal transporter 1 (DMT1) expression was significantly increased, and Prussian blue staining, ferrous iron (Fe^{2+}), MDA, and GSH level detection demonstrated that ferroptosis occurred in the infraction myocardium and in cardiomyocyte following hypoxia-induced injury. Overexpression of DMT1 promoted H/R-induced myocardial cell ferroptosis, while knockdown of DMT1 significantly inhibited the ferroptosis. HUCB-MSCs-derived exosomes inhibited ferroptosis and reduced myocardial injury, which was abolished in exosome with miR-23a-3p knockout. Moreover, dual luciferase reporter assay confirmed that DMT1 was a target gene of miR-23a-3p. In conclusion, HUCB-MSCs-exosomes may suppress DMT1 expression by miR-23a-3p to inhibit ferroptosis and attenuate myocardial injury.

Keywords HUCB-MSCs · Exosome · MiR-23a-3p · Acute myocardial infarction · Ferroptosis

Introduction

Acute myocardial infarction (AMI) usually causes myocardial damage and heart failure due to a sudden decrease in oxygen and blood supply and is one of the main causes of morbidity and mortality (Davidson et al. 2019). Ferroptosis is an oxidized, iron-dependent form of cell death which is different from necrosis, apoptosis, and autophagy. The intracellular glutathione (GSH)–dependent antioxidant defense system is inactivated, resulting in the accumulation of toxic lipid reactive oxygen species (ROS), which leads to ferroptosis. It is reported that ferroptosis could occur in ischemia-reperfusion (I/R) injury, cancer, etc. (Dixon et al. 2012). Although it is well known that cardiomyopathy is related to iron overload, less attention has paid to the role of iron in I/R. Ischemia itself will lead to the accumulation of iron in the myocardium, and the increased in the iron content of the myocardium will make the I/R injury worse. Iron as a free radical increases myocardial oxidative stress during I/R. Even though

Electronic supplementary material The online version of this article (https://doi.org/10.1007/s10565-020-09530-8) contains supplementary material, which is available to authorized users.

Y. Song
Department of Anesthesiology Department, Henan Provincial People's Hospital and Fuwai Central China Cardiovascular Hospital, Zhengzhou, Henan 461464, People's Republic of China
e-mail: zhenweig@yeah.net

B. Wang · X. Zhu · J. Hu · J. Sun · J. Xuan · Z. Ge
Department of Cardiovascular Surgery, Henan Provincial People's Hospital and Fuwai Central China Cardiovascular Hospital, 1 Fuwai Road, Zhengzhou, Henan 461464, People's Republic of China

the accumulation of iron in ischemic myocardium is a regulatory process, there is no relevant information on the regulation of iron homeostasis during myocardial ischemia. Simonis' s research suggested that iron metabolism was an important factor for ischemic injury after myocardial infarction (Simonis et al. 2010).

A recent study showed that ferroptosis was an important form of cardiomyocytes death (Baba et al. 2018). At present, the research on ferroptosis in heart disease had been gradually carried out. I/R injury caused ferroptosis in cardiomyocytes and cardiomyopathy, and the mechanism was that exposure of heart tissue to transient IR could lead to NRF2-dependent HMOX1 upregulation and heme degradation, together with iron overload and related lipid peroxidation which were hallmarks of ferroptosis increased (Fang et al. 2019; Conrad and Proneth 2019). Li et al. (2019a, b) uncovered that ferroptosis orchestrated neutrophil recruitment to injured myocardium, and which initiated inflammatory responses after cardiac transplantation. Gao et al. (2015) found that inhibiting ferroptosis by inhibiting glutamine metabolism could reduce heart injury triggered by I/R. Baba et al. (Dixon et al. 2012) demonstrated that ferroptosis was an important type of cardiomyocyte death, and knockout of mTOR could protect myocardial cell from excess iron and ferroptosis by regulating ROS production. Therefore, we speculated that ferroptosis played an important role in AMI.

The MSCs derived from human umbilical cord (HUCB-MSCs) have a promising application prospect because of their lower immunogenicity, higher proliferation factors, and higher transfection efficiency. It has been reported that exosomes derived from HUCB-MSCs relieved AMI injury (Zhao et al. 2015). So, does MSCs exosome have a regulatory effect on ferroptosis in AMI? As a key component of the complex physiological process, the divalent metal transporter DMT1 (Slc11a2) could regulate iron levels in the body. In mammals, the DMT1was a $Fe^{(2+)}$ transporter and essential for proper maintenance of iron homeostasis (Pujol-Giménez et al. 2017; Xue et al. 2016; Chia-Yu and Knutson 2013). Until now, there was no direct evidence to show the correlation between DMT1 expression and AMI. Ferguson et al. (2018) discovered that miR-23a-3p was highly expressed in exosomes of BMSCs. According to starbaseV2.0 software predictive analysis, miR-23a-3p could target Slc11a2, suggesting that MSC-exosome may inhibit the ferroptosis of myocardial cells after AMI and promote the repair of injury by secreting miR-23a-3p. Therefore, the present study aimed to explore whether HUCB-MSCs-exosomes inhibited ferroptosis by miR-23a-3p/DMT1 axis to attenuate myocardial injury in AMI mice.

Here, we investigated the expression and role of DMT1 in vitro and in vivo AMI models. HUCB-MSCs-exosomes were incubated with myocardial cell after H/R treatment, or administrated after ligation of the left anterior descending (LAD) coronary artery in mice. Our results indicated that DMT1 was significantly upregulated at 24 h after the establishment of AMI model, overexpression of DMT1 promoted H/R-induced myocardial cell ferroptosis, and knockdown of DMT1 significantly inhibited the ferroptosis. Moreover, HUCB-MSCs-derived exosomes inhibited ferroptosis and reduced myocardial injury, which was abolished in exosome obtained from HUCB-MSCs with miR-23a-3p inhibition. Our studies suggest that exosomes from HUCB-MSCs suppressed the ferroptosis of cardiomyocyte to mediate myocardial repair in AMI mice via delivering miR-23a-3p.

Material and method

Preparation of HUCB-MSCs

HUCB-MSCs were isolated from normal human umbilical cord blood that was provided by Department of Maternity, Henan Provincial People's Hospital and Fuwai Central China Cardiovascular Hospital. The written informed consent was obtained from the puerpera and their families. The expression rates of CD44, CD29, CD105, CD34, and CD45 antigen were detected by flow cytometry. The HUCB-MSCs were respectively cultured with adipogenic differentiation kit and osteogenic differentiation kit (Invitrogen, Carlsbad, CA, USA) and stained with oil red O and Alizarin Red to observe lipid droplets in adipocytes and calcium deposition in bone cells.

Isolation and characterization of exosomes

Before exosome isolation, the MSCs were cultured in exosome-free medium, and the exosome were isolated using the Total Exosome Isolation Reagent (Invitrogen, Life Technologies). Collected cell culture supernatant was centrifuged to remove debris and cells (2000×*g*, 30 min). Before incubation overnight at 4 °C, adding

exosome isolation agent into supernatant, the mixture was centrifuged (10,000×*g*, 1 h) to obtain pellet exosomes, which were then re-suspended in PBS. The conditioned supernatant of HUCB-MSCs or interfered by miR-23a-3p inhibitor were collected and centrifuged. After the removal of dead cells and cell debris, the exosomes were separated by ultracentrifugation and re-suspended in NCI-Exo and miR-23a-3pI-Exo. Exosomes were identified by western blot, transmission electron microscope (HITACHI, H-600IV, Tokyo, Japan), and Nanoparticle Tracking Analysis (Malvern Instruments, UK).

Labeled exosome

The PKH67 Green Fluorescent Cell Linker Kit (Sigma-Aldrich) was used to mark the exosome. Firstly, the exosomes were incubated with diluent C and PKH67 dye for 5 min. To bind excess dye, we add 1% BSA into that mixture. And then, we quickly remove unmerged dye from the labeled exosome preparation by an exosome spin columns (Invitrogen). Myocardial cells were cultured in medium containing PKH67 exosomes. After fixation, the cells were stained (DAPI) and photographed under a confocal microscope.

Myocardial cell isolated, transfected, and incubated

Whole hearts were isolated from embryonic mice. The minced hearts tissue was then incubated with 1 mg/ml collagenase II (Invitrogen, USA) at 37 °C and shaken (100 rpm, 5 min). The collected supernatant (containing separated cells) was centrifuged, and then removed the supernatant and re-suspended the cells in Gey's solution for 10 min to lyse the red blood cells. Cells were collected and centrifuged, re-suspended in buffer, and counted using a hemocytometer. In order to construct an in vitro myocardial H/R model, cells were incubated in a 37 °C hypoxic incubator (95% N_2 and 5% CO_2) for 6 h. Then, the incubation conditions were converted to normal (95% O_2, 5% CO_2, 37 °C) for one day. The isolated myocardial cells were transfected with lentivirus which is carrying DMT1-expressing sequence/DMT1 interference sequence or negative control, and incubated with exosome. After treatment, the myocardial cells were collected and analyzed by qRT-PCR, western blot, et al.

AMI model and infusion of exosomes

All experimental protocols were preapproved by the Experimental Animal Ethic Committee of Henan Provincial People's Hospital and Fuwai Central China Cardiovascular Hospital. A total of 72 C57BL/6J mice (six animals per group) were obtained from the Shanghai Laboratory Animals Center. The mouse model of AMI was performed by permanent ligation of the LAD coronary artery. PBS or exosomes (5ug, in 20 μl PBS) was injected into the border zone of infarcted heart at three sites.

Prussian blue staining

Localization of ferric iron in tissue sections or cell was carried out by Prussian blue. For cell, the treated cells were fixed with 4% paraformaldehyde for 15 min. Prussian blue staining solution was added into cell to incubate for 30 min, and washed with deionized water for 2–3 times. Then, the cell was re-dyed with Prussian solution for 30 s again, and washed with water again. After drying, the cell was placed under a light microscope to observe the blue particles. For tissue, the heart slices were dewaxed and re-hydrated with alcohol. Later, the slides were immediately transferred to the working staining solution at room temperature for 20 min, rinsed in distilled water, and then counterstained with nuclear-fast red. At last, the slides were dehydrated with ethanol, clarified with xylene, and mounted. Then, the stained sections were observed under an optical microscope.

Iron assay

The determination of intracellular ferrous iron level (Fe^{2+}) uses the iron assay kit (#ab83366, Abcam). Firstly, samples were collected, washed with cold PBS, and homogenized in iron assay buffer, then iron reducer was added in to the collected supernatant, mixed, and incubated. Finally, iron probe was added, mixed, and incubated for 1 h, and the content was immediately measured on a colorimetric microplate reader (the absorbance is 593 nm, $OD_{593\ nm}$).

MDA, GSH, and GPX4 analysis

The relative concentration of MDA was determined using a Lipid Peroxidation Assay Kit (#ab118970, Abcam). The MDA in the sample reacts with TBA to

form a MDA-TBA adduct, which was further quantified by colorimetrically ($OD_{532\ nm}$). GSH ELISA kits and GXP4 ELISA kits (mlbio, China) were used to measure GSH and GPX4 levels in tissues or cells.

qRT-PCR analysis

Myocardial tissues or cells were treated with TRIzol (Invitrogen), and total RNA was extracted using an RNA extraction kit (TaKaRa). After reverse transcription of RNA into cDNA, PCR was performed to amplify the target gene. DMT1, F: 5′-GTGC GGGAAGCCAATAAGTA-3′,R: 5′-TCAC TGGGAAAGAGGTCAGC′; the matured mouse miR-23a-3p expression was determined by a stem-loop real-time PCR system (Maxima™ SYBR Green qPCR Master Mix and StepOne™ sequence detector). The primer of miR-23a-3p, F: 5′-GTCG TATCCAGTGCAGGGTCCGAGGTATTCGC ACTGGATACG-AGGAAATCC-3′, R: 5′-TCAG TCGATCACATTGCCAG-3′; change in level of expression was compared with GAPDH (for DMT1 expression) and U6 (for miR-23a-3p expression).

Western blot analysis

The protein were fractionated by SDS-PAGE and blotted to PVDF (Millipore). Membranes were blocked for 1 h using 5% nonfat milk. Then, they were probed overnight with the following primary antibodies at 4 °C: DMT1 (1:1000 dilution), GPX4 (1:500 dilution), and β-actin (1:1000 dilution). After incubation with the primary antibodies, membranes were incubated with secondary antibody for 1 h. The protein bands were quantified by measuring the band intensity in each group.

Cell viability

The CCK8 assay was used to determine the cell viability. Briefly, the treated cell was collected, and the culture supernatants were transformed into 10% CCK-8 fresh medium. With the background reading taken into account, the absorbance at 450 nm, which represents cell viability, was measured in a multimode microplate reader.

Quantification of ROS

The Reactive Oxygen Species assay kit (Beyotime Institute of Biotechnology) was used to monitor the generation of intracellular ROS by fluorescent probe DCFH-DA. DCFH-DA is converted to DCFH and then to fluorescent DCF by intracellular esterase and ROS, respectively. In brief, the cells were incubated with DCFH-DA, subsequently washed with PBS, and then analyzed by a flow cytometer excited at 488 nm and emitted at 525 nm (Beckman Coulter, Inc.).

Cell apoptosis

The flow cytometry was used to determine the cell apoptosis. The treated cell were collected, stained with Annexin-V and PI (eBioscience, USA), and detected by flow cytometry. The data were analyzed by FlowJo software.

Luciferase reporter assay

The binding sites between the 3′UTR of DMT1and miR-23a-3p were identified by Starbase. Their target relationship was proved by the luciferase reporter assay. Firstly, the DMT1-3′-UTR was amplified from human cDNA. The wide-type fragment containing the predicted miR-23a-3p binding site and its mutant fragment was obtained from 3′-UTR of DMT1. The human embryonic kidney cell line (HEK293T) was selected in this assay. When the cell that seeded in 24-well plates reached to 70 to 80% confluence, the miR-23a-3p mimic, inhibitor, and wild-type or mutant reporter (GenePharma, Shanghai, China) were co-transfected into HEK293T. Twenty-four hours after transfection, the luciferase activity was measured by the dual luciferase assay kit (Promega).

TTC staining for infarct size

After the mice were killed, the hearts were removed, washed, and placed in a heart cutting groove. Then, they were put in the refrigerator (− 20 °C, 2 h). Heart slices were taken in units of 2 mm and placed in TTC staining solution and incubated (37 °C, 30 min). The results were observed and the ImageJ software was used to measure the area of myocardial infarctionthey.

HE staining analysis

The heart tissues were embedded in paraffin after fixation with 4% paraformaldehyde, and dehydrated in ethanol. After paraffin embedding, the sample was cut into 5-μm thick slices and stained wtih hemotoxylin and eosin staining for light microscopy.

TUNEL analysis

Cardiomyocyte apoptosis in heart tissue was detected by TUNEL assay. Five randomly selected fields in each sample were observed for counting TUNEL-positive cells and DAPI-stained nucleus.

Statistics

The experiment was repeated three times. All data are expressed as mean ± standard deviation (SD). Differences between two groups or multiple groups were analyzed by Student's *t* test and ANOVA, respectively. *p* values were calculated with Student's *t* test using GraphPad Prism software, and less than 0.05 were considered significant.

Results

Upregulated DMT1 expression and increased ferroptosis in AMI mice

AMI model of mice was established, and the left ventricular myocardial tissue was collected at 1 h, 4 h, 12 h, 24 h, and 48 h after operation. As the RT-PCR and western blot showed, DMT1 expression was obviously higher than the sham group at 24 h and 48 h in AMI mice, while the GPX4 protein expression was decreased (Fig. 1a, b). These data suggested that DMT1 was significantly upregulated at 24 h after the establishment of AMI model.

Using Prussian blue staining and iron assay kit, we found the increased iron deposition and ferrous iron (Fe^{2+}) level at 12 h, 24 h and 48 h in AMI mice (Fig. 1c, d). In addition, the MDA level was also increased at 24 h and 48 h in AMI mice, while the GSH level and GPX4 activity were both decreased at 24 h and 48 h in AMI mice (Fig. 1f, g). These data suggested that ferroptosis may occur in myocardial tissue at 24 h after LAD for AMI model.

Overexpression of DMT1 promoted H/R-induced cell ferroptosis

The myocardial cells isolated from neonatal mice were treated with H/R and transfected with lentivirus which was carrying DMT1-expressing sequence/DMT1 interference sequence or negative control. As expected, compared with the control group, DMT1 mRNA and protein expression level were both upregulated in H/R group (Fig. 2a, b). Under H/R treatment, the changes of cell viability assay and morphological revealed that overexpression of DMT1 further reduced cell viability, while knockdown of DMT1 obviously increased cell viability (Fig. 2c). Normal myocardial cells extended pseudopods in contact with each other in a network of radial arrangement, H/R treatment caused the synapses of the cells became thin, retracted and the cytoplasm shrunk. Under H/R treatment, overexpression of DMT1 further caused apoptosis with nuclear chromatin condensation and fragmentation as well as cell shrinkage, while knockdown of DMT1 obviously improved cytoplasm shrunk (Fig. 2d). As shown in Fig. 2g, h, the flow cytometric analysis data revealed that H/R induced cell apoptosis, and overexpression of DMT1 further aggravated the apoptosis, while knockdown of DMT1 significantly inhibited the apoptosis.

Next, we found that the intracellular ROS level, iron deposition, ferrous iron (Fe^{2+}), and MDA level were all increased in H/R group, and overexpression of DMT1 further increased H/R-induced ROS level, iron deposition, ferrous iron (Fe^{2+}), and MDA level, while knockdown of DMT1 significantly reduced H/R-induced ROS level, iron deposition, ferrous iron (Fe^{2+}), and MDA level (Fig. 2e–f, i–k). Moreover, the decreased GSH level and GPX4 activity was discovered in H/R group, and overexpression of DMT1 further decreased GSH level, while knockdown of DMT1 significantly increased GSH level (Fig. 2l). However, DMT1 had no significant effect on GPX4 activity (Fig. 2m). These data demonstrated that overexpression of DMT1 promoted H/R-induced cell ferroptosis, and knockdown of DMT1 significantly inhibited H/R-induced cell ferroptosis.

Isolation and identification of HUCB-MSCs and exosomes

To investigate the role of exosomes from HUCB-MSCs on myocardial cell ferroptosis, the HUCB-MSCs were

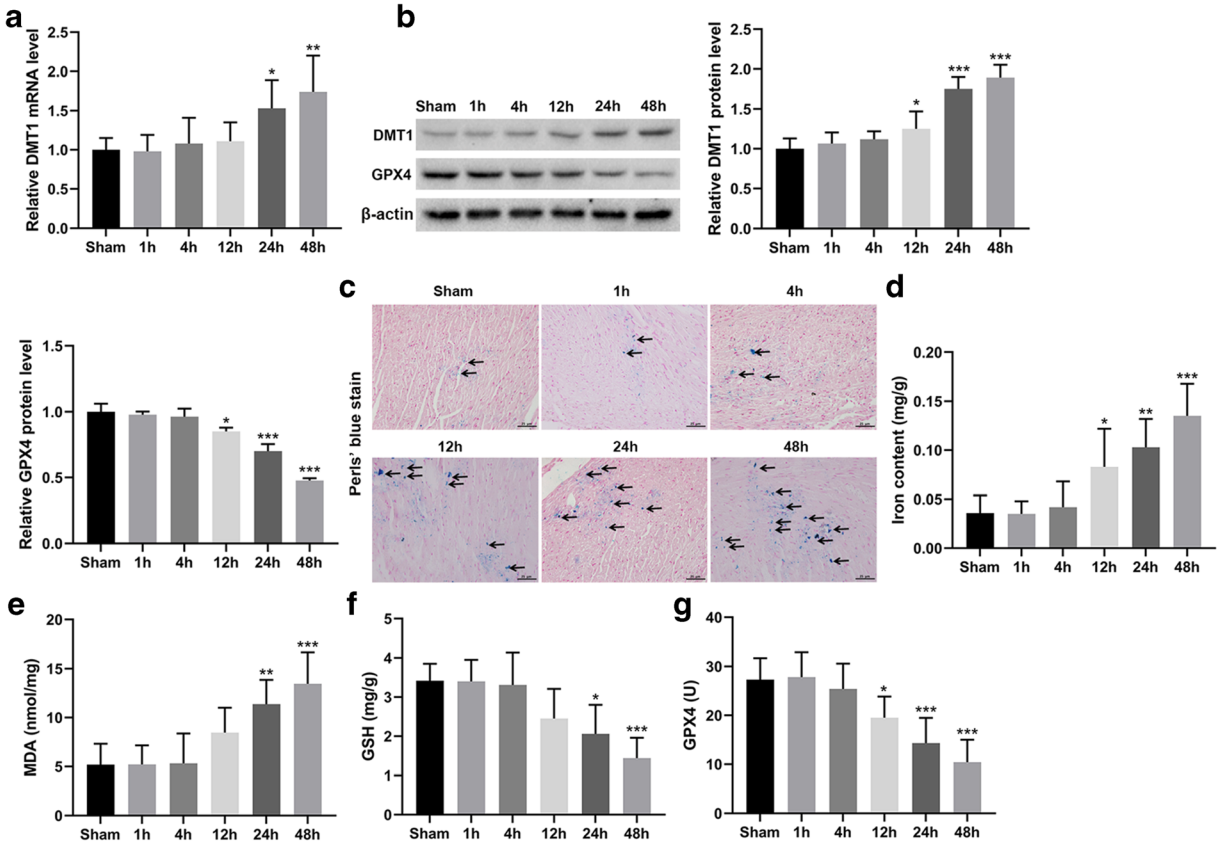

Fig. 1 Upregulated DMT1 expression and increased ferroptosis in AMI mice. AMI model of mice was established, and **a**, **b** the expression of DMT1 and GPX4 by RT-PCR and western blot, **c** the iron deposition by Prussian blue staining, **d** the ferrous iron (Fe^{2+}) level by iron assay kit, **e** the MDA level by a lipid peroxidation assay kit, **f** the GSH level by ELISA, and **g** the GPX4 activity by ELISA in myocardial tissue were detected at different time point. Six animals per group, $*p < 0.05$; $**p < 0.01$; $***p < 0.01$ vs sham

isolated and characterized. As the Fig. 3a and Supplementary Figure 1 showed, the expression rates of CD44, CD29, CD73, CD105, and CD90 antigen were greater than 94%, while the expression rates of CD45 and CD34 cells were both lower than 1%. The osteogenic and adipogenic differentiation experiment described in Fig. 3b showed the activity of HUCB-MSCs. As showed in Fig. 3c, d, the exosomes isolated from the conditioned supernatant of HUCB-MSCs was elliptical nanovesicles and the particle size distribution ranged from 0 to 400 nm. In addition, these collected exosome surface marker proteins (such as CD9 and CD63) were positive (Fig. 3e). All above, we identified that the particles derived from HUCB-MSCs were exosomes.

To prove the exosomes derived from HUCB-MSCs can change gene expression of myocardial cells, firstly, we have demonstrated that the exosomes could be absorbed into myocardial cells. HUCB-MSCs-exosomes labeled with PKH67 and be added into myocardial cell culture fluid. After incubation for 6 h as shown in Fig. 3f, most of myocardial cells obtained the PKH67-labeled exosomes, and HUCB-MSCs-exosomes were distributed similarly in the cytoplasm of myocardial cells.

HUCB-MSCs-derived exosomes deliver miR-23a-3p to inhibit ferroptosis

To study the effect of miR-23a-3p on the HUCB-MSCs-exosomes effect, the miR-23a-3p-deficient exosomes was obtained by transfecting miR-23a-3p inhibitor into HUCB-MSCs. Figure 4a shows the successful knockdown of miR-23a-3p in resultant exosomes. To further study the effect of the exosomes on myocardial cells ferroptosis, the H/R-induced myocardial cell was constructed to simulate in vitro AMI injury. Figure 4b

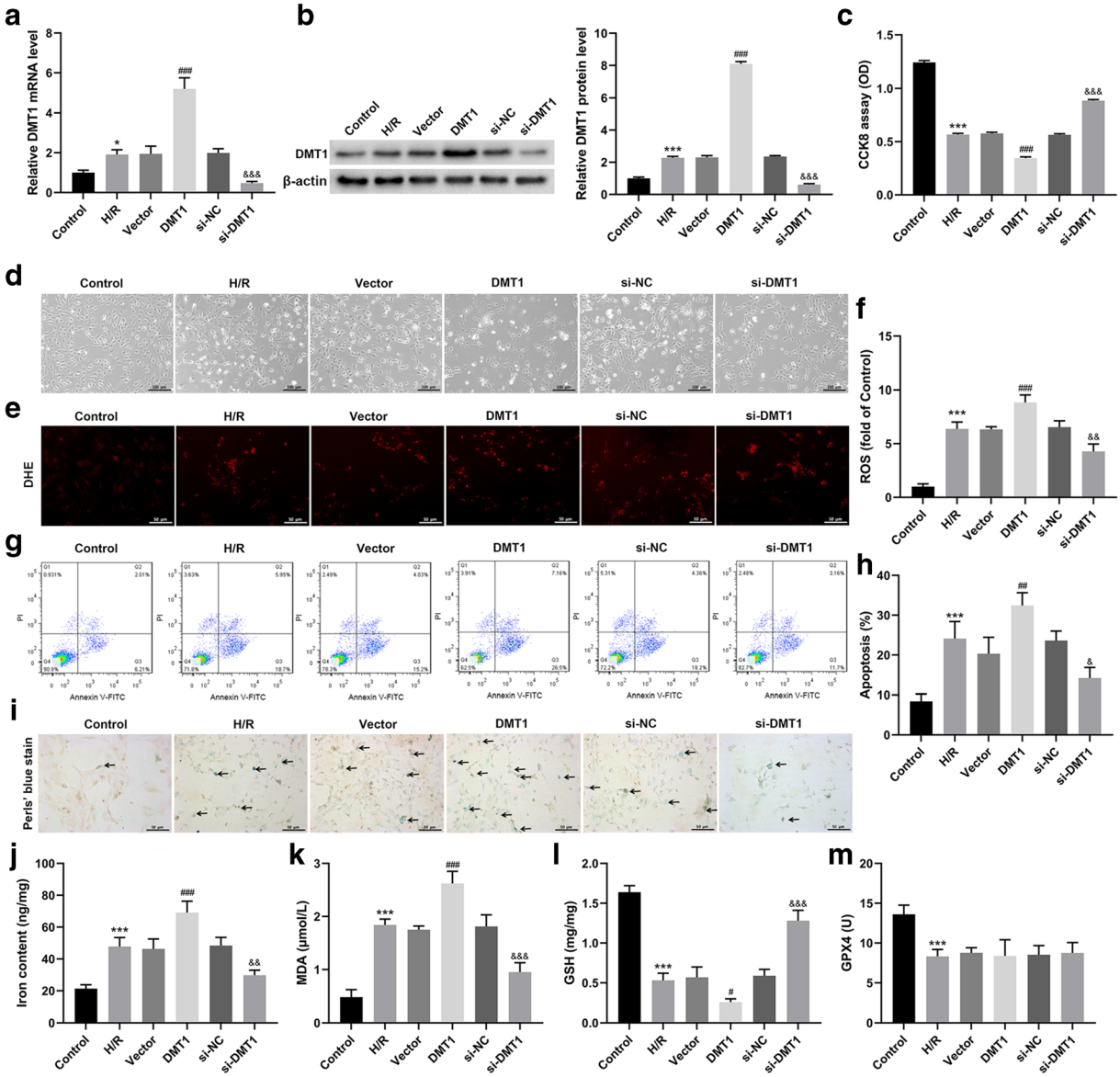

Fig. 2 The effect of DMT1 on myocardial cell ferroptosis. **a**, **b** The DMT1 expression in DMT1 overexpression and knockdown cells. **c** The cell viability by CCK8 assay. **d** The cellular morphology by phase contrast microscopy. **e**, **f** The intracellular ROS level by DHE fluorescence. **g**, **h** The cell apoptosis rate by flow cytometry. **i** The iron deposition by Prussian blue staining. **j** The ferrous iron (Fe^{2+}) level by iron assay kit. **k** The MDA level by a lipid peroxidation assay kit. **l** The GSH level by ELISA. **m** The GPX4 activity by ELISA. The experiment was repeated three times. $^{*}p < 0.05$; $^{***}p < 0.01$ vs control. $^{\#}p < 0.05$; $^{\#\#}p < 0.01$; $^{\#\#\#}p < 0.01$ vs vector. $^{\&}p < 0.05$; $^{\&\&}p < 0.01$; $^{\&\&\&}p < 0.01$ vs si-NC

shows that the expression of miR-23a-3p was decreased in H/R-induced cell, while it was increased in myocardial cell co-cultured with the exosomes. The DMT1 mRNA and protein expression was contrary to that of miR-23a-3p in myocardial cell co-cultured with HUCB-MSCs-exosomes (Fig. 4c, d). As we have known that overexpression of DMT1 further reduced cell viability and GSH level, and increased cell apoptosis, intracellular ROS level, iron deposition, ferrous iron (Fe^{2+}), and MDA level in H/R-treated myocardial cell. Here, all the results shown in Fig. 4e–m have the same tendency of changes with DMT1 expression, which suggested that DMT1 was one of the key targets for HUCB-MSCs-derived exosomes deliver miR-23a-3p to inhibit

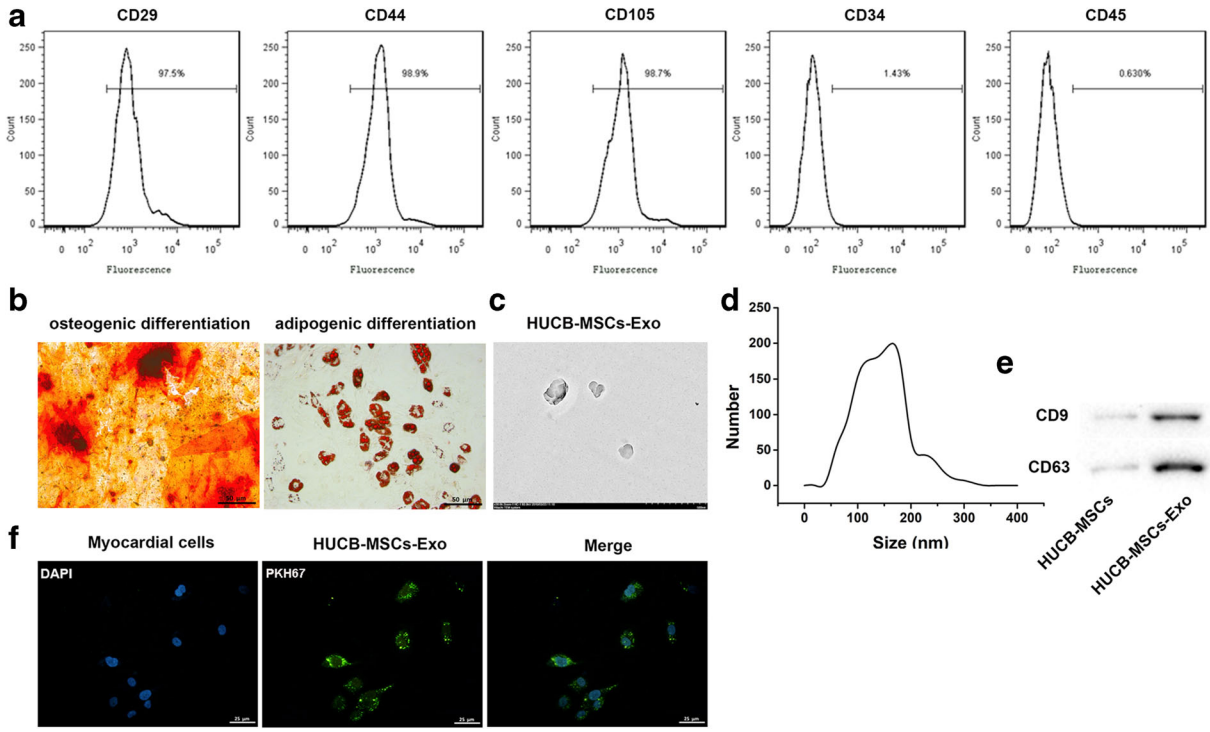

Fig. 3 Isolation and identification of HUCB-MSCs and derived exosomes. **a** The characteristics of HUCB-MSCs by flow cytometry. **b** The osteogenic and adipogenic differentiation of HUCB-MSCs by alizarin red staining and oil red O staining. **c** The exosome by TEM. **d** The particle size of exosomes by NTA. **e** The exosome marker expression by western blot. **f** The exosomes uptake into myocardial cells by LSCM

ferroptosis. Also, HUCB-MSCs-exosomes had no significant effect on GPX4 activity (Fig. 4n).

Moreover, the miR-23a-3p-depletion HUCB-MSCs-exosomes played a weak inhibitory role in myocardial cells ferroptosis, showing reduced cell viability and GSH level, and increased cell apoptosis, intracellular ROS level, iron deposition, ferrous iron (Fe^{2+}), and MDA level compared with NCI-Exo group (Fig. 4e–m). The data implied that HUCB-MSCs-derived exosomes deliver miR-23a-3p to inhibit ferroptosis.

HUCB-MSCs-derived miR-23a-3p-expressing exosomes inhibited ferroptosis by targeting DMT1

The Starbase software has predicted the bind relationship of the miR-23a-3p and 3′UTR of the DMT1. As shown in Fig. 5a, the cell transfected with miR-23a-3p mimic has decreased the luciferase activity in DMT1-WT co-transfected system, while there was no obvious change in DMT1-MUT co-transfected system, suggesting the direct binding between the miR-23a-3p and DMT1. The myocardial cells were infected with overexpressed DMT1 lentivirus while incubating with HUCB-MSCs-exosomes. The DMT1 mRNA and protein expression levels were both decreased in Exo-Vector group and increased in Exo + DMT1 group, suggesting the negative regulatory effect of HUCB-MSCs-exosomes on DMT1 expression (Fig. 5b). After infected with overexpressed DMT1 lentivirus, the increased cell viability and GSH level induced by HUCB-MSCs-exosomes were both decreased, and the decreased cell apoptosis, intracellular ROS level, iron deposition, ferrous iron (Fe^{2+}), and MDA level were all increased (Fig. 5c–k), indicating that HUCB-MSCs-derived miR-23a-3p-expressing exosomes inhibited ferroptosis by targeting DMT1.

HUCB-MSCs-exosomes suppressed the ferroptosis of cardiomyocyte in AMI mice

To study the protective mechanism of exosomes of HUCB-MSCs on AMI mice, TTC staining showed an alleviated infarct size in HUCB-MSCs-exosomes administration, while miR-23a-3pI-Exo administration

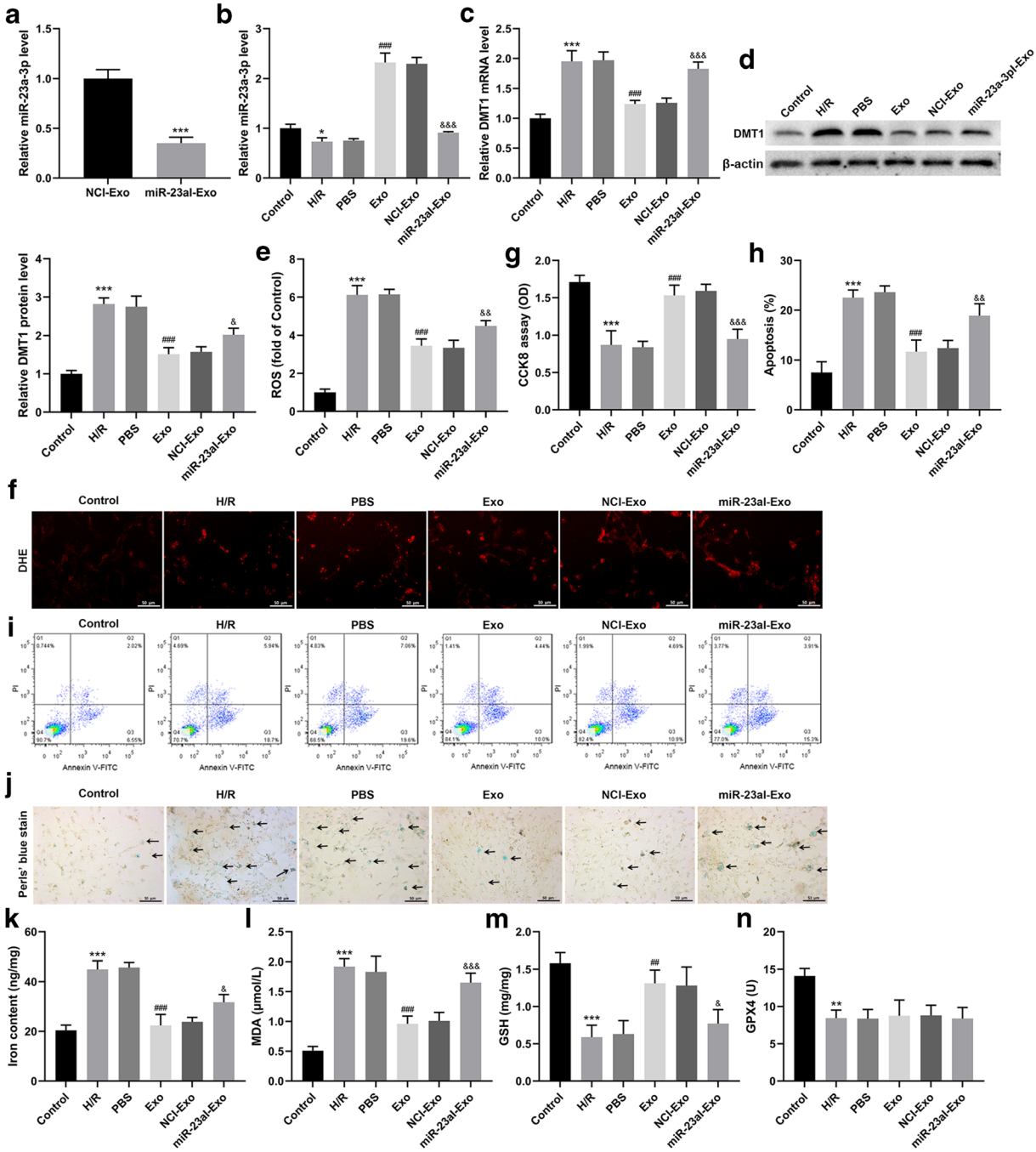

Fig. 4 HUCB-MSCs-derived exosomes inhibited myocardial cell ferroptosis through miR-23a-3p. **a** The miR-23a-3p expression by RT-PCR in exosome derived from HUCB-MSCs transfected with miRNA inhibitor NC or miR-23a-3p inhibitor, named NCI-Exo and miR-23a-3pI-Exo, respectively. **b** The miR-23a-3p expression by RT-PCR in myocardial cells with H/R and exosome treatment. **c**, **d** The DMT1 mRNA and protein expression by RT-PCR and western blot in myocardial cells with H/R and exosome treatment. **e**, **f** The intracellular ROS level by DHE fluorescence. **g** The cell viability by CCK8 assay. **h**, **i** The cell apoptosis rate by flow cytometry. **j** The iron deposition by Prussian blue staining. **k** The ferrous iron (Fe^{2+}) level by iron assay kit. **l** The MDA level by a lipid peroxidation assay kit. **m** The GSH level by ELISA. **n** The GPX4 activity by ELISA. The experiment was repeated three times. $^{*}p < 0.05$; $^{**}p < 0.01$; $^{***}p < 0.01$ vs control. $^{\#\#}p < 0.01$; $^{\#\#\#}p < 0.01$ vs PBS. $^{\&}p < 0.05$; $^{\&\&}p < 0.01$; $^{\&\&\&}p < 0.01$ vs NCI-Exo

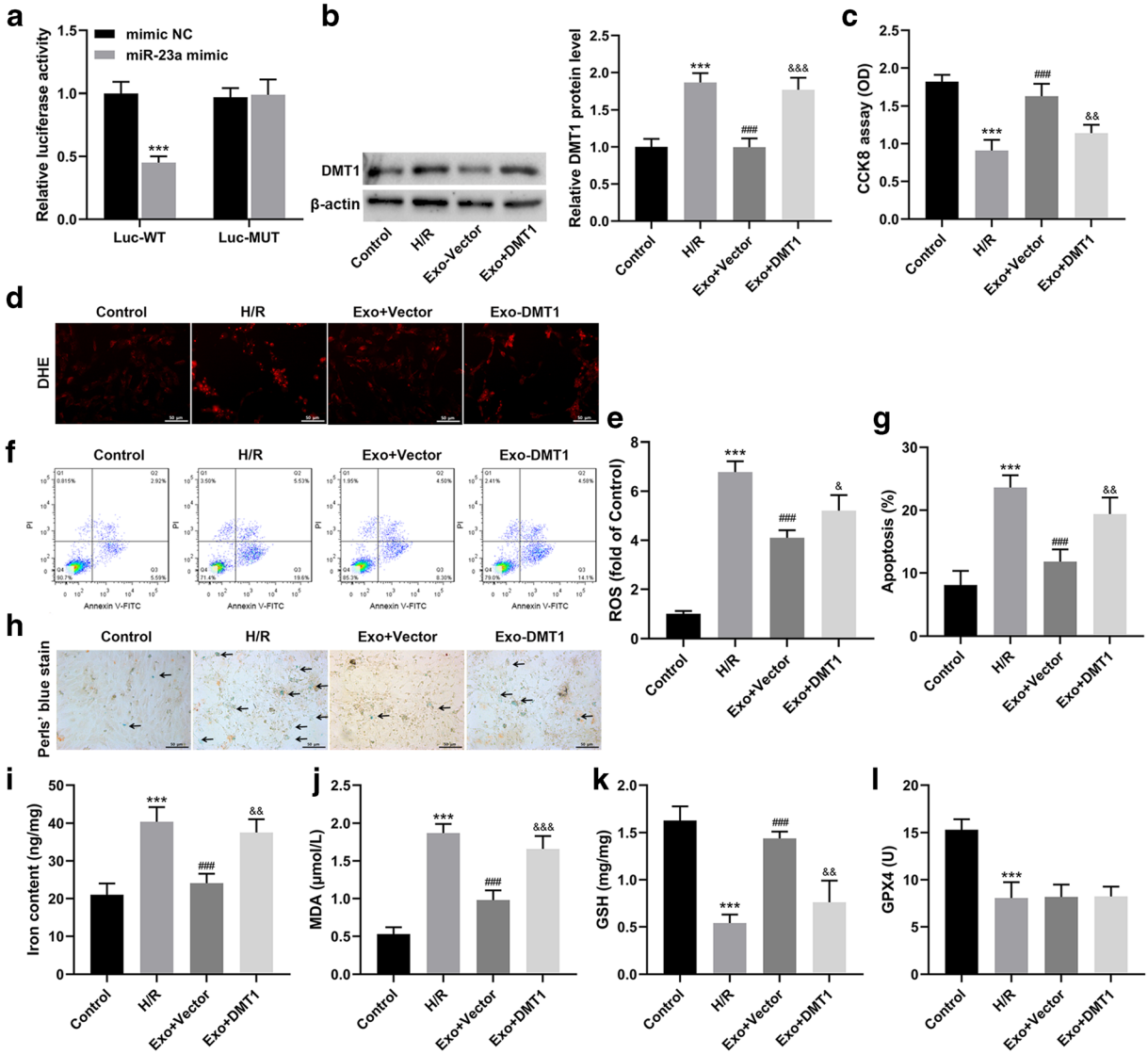

Fig. 5 HUCB-MSCs-derived miR-23a-3p-expressing exosomes inhibited myocardial cells ferroptosis by targeting DMT1. **a** The direct binding of microRNA-23a-3p and DMT1 was verified by luciferase activity assay. The myocardial cells were treated with H/R, exosome and overexpression DMT1, and then **b** the DMT1 expression by western blot, **c** the cell viability by CCK8 assay, **d**, **e** the intracellular ROS level by DHE fluorescence, **f**, **g** the cell apoptosis rate by flow cytometry, **h** the iron deposition by Prussian blue staining, **i** the ferrous iron (Fe^{2+}) level by iron assay kit, **j** the MDA level by a lipid peroxidation assay kit, **k** the GSH level by ELISA, **l** the GPX4 activity by ELISA. The experiment was repeated three times. $^{***}p < 0.01$ vs mimic NC or control. $^{\#\#\#}p < 0.01$ vs H/R. $^{\&}p < 0.05$; $^{\&\&}p < 0.01$; $^{\&\&\&}p < 0.01$ vs Exo + Vector

had significantly weakened role on alleviating infarct size in AMI mice (Fig. 6a). HE staining showed that myocardial structure was normal with regular arrangement, transverse striations of myocardium were clear, cytoplasm was not hyperchromatic, nucleus size was normal, and chromatin was evenly distributed in sham group. In AMI model group, the pathological changes of myocardial tissue were very obvious, the myocardial fiber cells were arranged disorderly and sparse, and severe swelling occurred. Cardiac cells with enhanced eosinophilic cytoplasm were seen scattered in the tissues. Patchy and focal necrosis of myocardium is seen occasionally. The horizontal striations of cardiac muscle cells disappeared, and a certain number of cardiac nuclei pyknosis and fragmentation, severe dissolution disappeared. The interstitial infiltration of cardiomyocytes

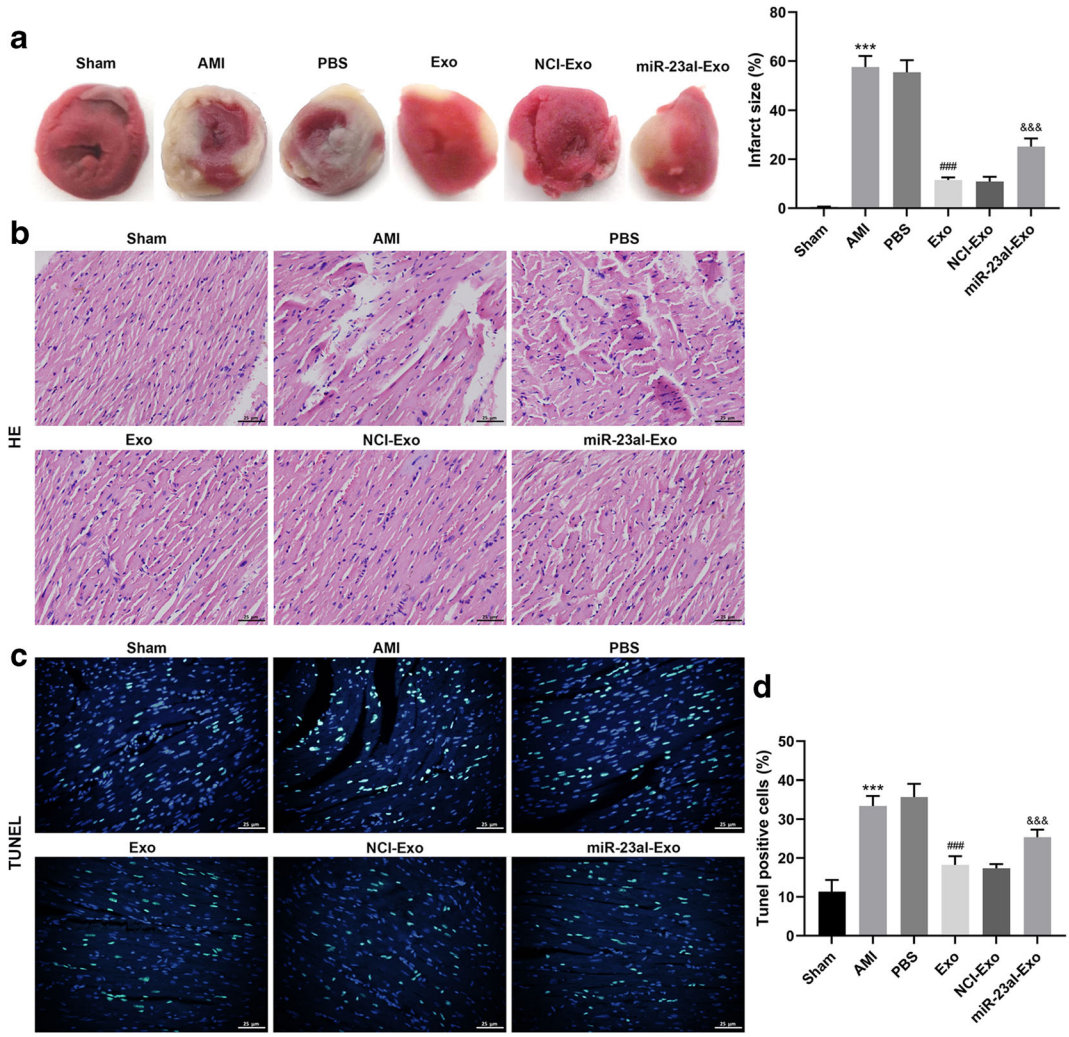

Fig. 6 HUCB-MSCs-exosomes reduced myocardial injury in AMI mice. **a** The infarct area by Evans Blue and TTC double staining. **b** The myocardial pathological morphology by HE staining. **c** The cell apoptosis in cardiac tissue by TUNEL. Six animals per group, $^{***}p < 0.01$ vs sham. $^{\#\#\#}p < 0.01$ vs PBS. $^{\&\&\&}p < 0.01$ vs NCI-Exo

was rich in inflammatory cells. Compared with the AMI group, the pathological changes was alleviated; the arrangement of muscle fibers was relatively regular. In addition, the swelling of cells was alleviated, flake and focal necrosis and myocardial dissolution were reduced, myocardial fibrous rupture was relatively rare, and the infiltration of inflammatory cells was reduced. HUCB-MSCs-exosomes administration alleviated myocardial injury, while miR-23a-3pI-Exo administration had significantly weakened role on alleviating myocardial damage in AMI mice (Fig. 6b). In order to analyze the status of cardiomyocytes apoptosis, the hearts were treated with TUNEL staining. We found that the proportion of TUNEL-positive cells in heart tissues of AMI mice was significantly increased, and the implantation of HUCB-MSCs-exosomes can eliminate this phenomenon. However, miR-23a-3pI-Exo transplantation has a higher apoptosis index than NCI-Exo transplantation (Fig. 6c). The results indicated that HUCB-MSCs-exosomes reduced myocardial injury in AMI mice.

As expected, exosomes of HUCB-MSCs obviously inhibited DMT1 expression, iron deposition, ferrous iron (Fe^{2+}), and MDA level, and upregulated GSH level, but the role of miR-23a-3pI-Exo on these was obvious weakened (Fig. 7a–e). In addition, HUCB-MSCs-exosomes had no significant effect on GPX4 activity in AMI mice (Fig. 7f). These results indicated that exosomes of HUCB-MSCs suppressed the ferroptosis

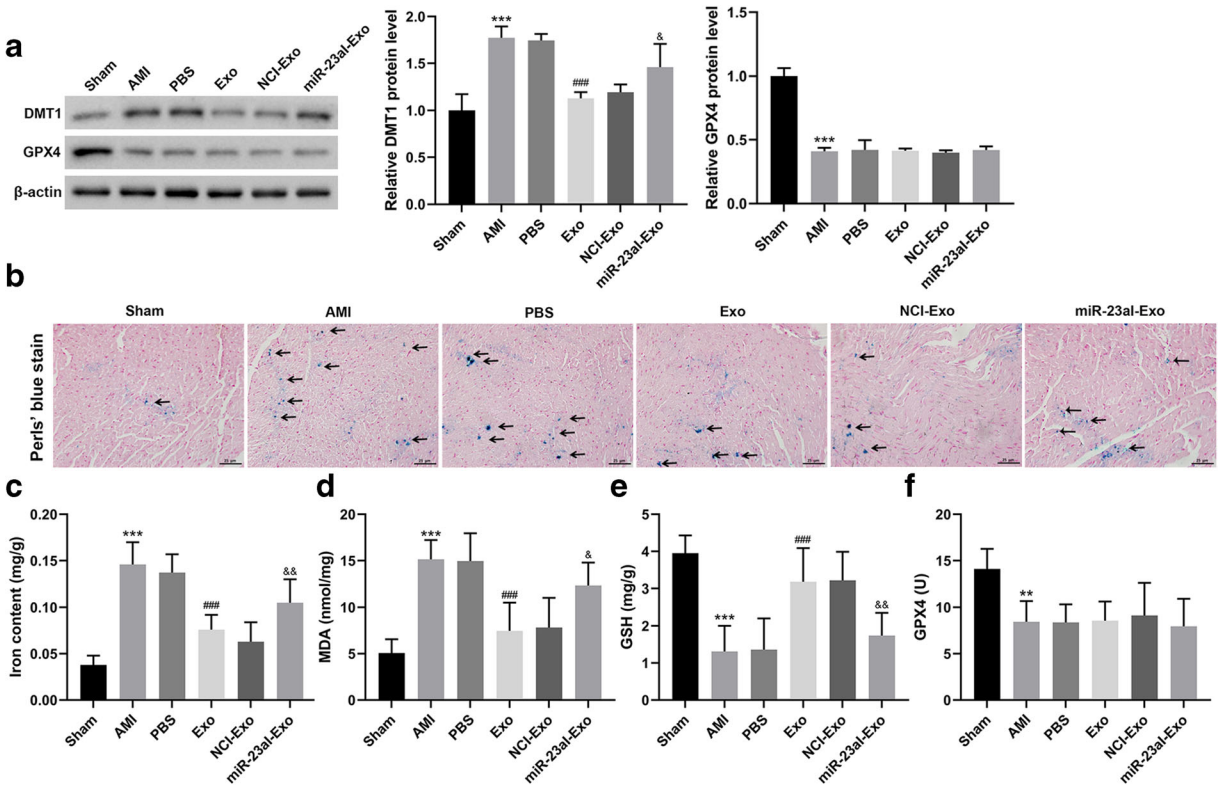

Fig. 7 HUCB-MSCs-exosomes suppressed the myocardial cells ferroptosis in AMI mice. **a** The DMT1 and GPX4 protein expression in cardiac tissue by western blot. **b** The iron deposition by Prussian blue staining. **c** The ferrous iron (Fe^{2+}) level by iron assay kit. **d** The MDA level by a lipid peroxidation assay kit. **e** The GSH level by ELISA. **f** The GPX4 activity by ELISA. Six animals per group, $^{**}p < 0.01$, $^{***}p < 0.01$ vs sham. $^{\#\#\#}p < 0.01$ vs PBS. $^{\&}p < 0.05$; $^{\&\&}p < 0.01$ vs NCI-Exo

of cardiomyocyte in AMI mice via delivering miR-23a-3p.

Discussion

Iron is the basic element of almost all organisms as it is involved in various metabolic processes, such as electron transport, DNA synthesis, and oxygen transport. Ferroptotic death is morphologically, biochemically, and genetically distinct from various forms of necrosis, apoptosis, and autophagy. As shown in several studies, ferroptosis was an important form of cell death in cardiomyocytes, and I/R injury caused ferroptosis in cardiomyocytes (Baba et al. 2018; Fang et al. 2019; Conrad and Proneth 2019). In this study, we found the increased iron deposition and ferrous iron (Fe^{2+}) level in AMI mice. In addition, the MDA level was also increased, while the GSH level and GPX4 activity were both decreased in AMI mice, suggesting that ferroptosis occurred in myocardial tissue of AMI model.

As a proton-coupled metal-ion transport protein, DMT1 was a key modulator of (non)transferrin-bound iron homeostasis. Upregulated DMT1 was association with ferroptosis according to the recent reported references (Yu et al. 2019; Li et al. 2019a, b; Núñez and Hidalgo 2019). DMT1 was a ferrous iron importer and plays a key role in iron uptake, as well as iron translocation from the endosome (Hubert and Hentze 2002). Du et al. (2016) have reported that decreased DMT1 expression could block iron influx. Here, DMT1 was significantly upregulated in myocardial tissue of the AMI mice model, overexpression of DMT1 promoted H/R-induced cell ferroptosis, and knockdown of DMT1 significantly inhibited H/R-induced cell ferroptosis. The present results agreed with the ones in the literature.

Emerging evidence suggested that MSCs-derived exosomes were the ideal candidate for mRNA delivery, which can be used in applications for AMI therapy (Huang et al. 2019; Bian et al. 2014). miR-23-3p was reported to be one of the enriched miRNAs in MSCs-derived exosomes (Ferguson et al. 2018). Zhao and

colleagues (Zhao et al. 2014) uncovered that miR-23-3p could protect neuronal cells from oxidative stress injury in experimental ischemic stroke. This article had demonstrated that the miR-23a-3p could also be as an antioxidative factor in H/R-induced myocardial cell, showing reduced intracellular ROS level in HUCB-MSCs-exosome group, but a weak inhibitory role on intracellular ROS level in miR-23a-3p-depletion HUCB-MSCs-exosomes group. In addition to the weakened inhibition of ROS level, the inhibition role of HUCB-MSCs-exosomes on iron deposition, ferrous iron (Fe^{2+}), and MDA level were also significantly weakened in H/R-induced cell, suggesting exosomes derived from HUCB-MSCs protected cell against H/R-induced ferroptosis via carrying miR-23a-3p.

As a key regulator of the antioxidant defense mechanism, the increased evidence suggested that NRF2 could be against myocardial I/R damage; many cardioprotective drugs could reduce I/R-induced oxidative stress via activating Nrf2/ARE pathway. In this study, HUCB-MSCs-derived miR-23a-3p-expressing exosomes could alleviate H/R-induced oxidative stress, but not by upregulating the activation of Nrf2/HO-1 (Supplementary Figure 4). MiRNAs could specific bind on 3′UTR of target mRNA to promote mRNA degradation (Chipman and Pasquinelli 2019). The dual luciferase reporter gene assay in this study demonstrated that DMT1 is a target gene of miR-23a-3p. And then, a reversed experiment by lentivirus-mediated DMT1 gene overexpression proved that HUCB-MSCs-derived miR-23a-3p-expressing exosomes inhibited ferroptosis by targeting DMT1, that DMT1 gene overexpression reversed the decreased ROS level, iron deposition, ferrous iron (Fe^{2+}), and MDA level by exosomes of HUCB-MSCs in H/R-induced myocardial cell.

In addition, GPX4 activity has significant decline in AMI mice model and H/R-induced myocardial cell. Overexpression or knockdown of DMT1 as well as HUCB-MSCs-exosomes had no effect on GPX4 activity. These results indicated that HUCB-MSCs-exosomes inhibited ferroptosis mainly through regulating iron metabolism pathway in AMI.

Conclusion

In conclusion, we demonstrated a new therapeutic effect of HUCB-MSCs-derived exosomes. HUCB-MSCs-exosomes could attenuate AMI mice myocardial injury through inhibiting ferroptosis by targeting DMT1 expression.

Authors' contributions ZG conceived and designed the analysis. YS, BW, XZ, JH, JS, JX, and ZG collected the data. YS, BW, XZ, and ZG contributed data or analysis tools. JH, JS, and JX performed the analysis. YS wrote the paper. All authors read and approved the manuscript.

Funding information This project was supported by The Key Science and Technology Research Projects in Henan Province (15210230149).

Compliance with ethical standards

Conflict of interest The authors declare that they have no conflict of interest.

References

Baba Y, Higa JK, Shimada BK, Horiuchi KM, Suhara T, Kobayashi M, et al. Protective effects of the mechanistic target of rapamycin against excess iron and ferroptosis in cardiomyocytes. Am J Physiol Heart Circ Physiol. 2018;314(3):H659–H68.

Bian S, Zhang L, Duan L, Wang X, Min Y, Yu H. Extracellular vesicles derived from human bone marrow mesenchymal stem cells promote angiogenesis in a rat myocardial infarction model. J Mol Med. 2014;92(4):387–97.

Chia-Yu W, Knutson MD. Hepatocyte divalent metal-ion transporter-1 is dispensable for hepatic iron accumulation and non-transferrin-bound iron uptake in mice. Hepatology. 2013;58(2):788–98.

Chipman LB, Pasquinelli AE. miRNA targeting: growing beyond the seed. Trends Genet. 2019;35(3):215–22.

Conrad M, Proneth B. Broken hearts: iron overload, ferroptosis and cardiomyopathy. Cell Res. 2019;29(4):263–4. https://doi.org/10.1038/s41422-019-0150-y.

Davidson SM, Ferdinandy P, Andreadou I, Bøtker HE, Heusch G, Ibáñez B, et al. Multitarget strategies to reduce myocardial ischemia/reperfusion injury: JACC Review Topic of the Week. J Am Coll Cardiol. 2019;73(1):89–99.

Dixon SJ, Lemberg KM, Lamprecht MR, Skouta R, Zaitsev EM, Gleason CE, et al. Ferroptosis: an iron-dependent form of nonapoptotic cell death. Cell. 2012;149(5):1060–72.

Du X, Xu H, Shi L, Jiang Z, Song N, Jiang H, et al. Activation of ATP-sensitive potassium channels enhances DMT1-mediated iron uptake in SK-N-SH cells in vitro. Sci Rep. 2016;6(undefined):33674.

Fang X, Wang H, Han D, Xie E, Yang X, Wei J, et al. Ferroptosis as a target for protection against cardiomyopathy. Proc Natl Acad Sci U S A. 2019;116(7):2672–80.

Ferguson SW, Wang J, Lee CJ, Liu M, Neelamegham S, Canty JM, et al. The microRNA regulatory landscape of MSC-derived exosomes: a systems view. Sci Rep. 2018;8(1):1419.

Gao M, Monian P, Quadri N, Ramasamy R, Jiang X. Glutaminolysis and transferrin regulate ferroptosis. Mol Cell. 2015;59(2):298–308.

Huang P, Wang L, Li Q, Tian X, Xu J, Xu J et al. Atorvastatin enhances the therapeutic efficacy of mesenchymal stem cells derived exosomes in acute myocardial infarction via up-regulating long non-coding RNA H19. Cardiovascular Research. 2019;undefined (undefined):undefined.

Hubert N, Hentze MW. Previously uncharacterized isoforms of divalent metal transporter (DMT)-1: implications for regulation and cellular function. Proc Natl Acad Sci U S A. 2002;99(19):12345–50. https://doi.org/10.1073/pnas.192423399.

Li LB, Chai R, Zhang S, Xu SF, Zhang YH, Li HL et al. Iron exposure and the cellular mechanisms linked to neuron degeneration in adult mice. Cells. 2019a;8(2):undefined.

Li W, Feng G, Gauthier JM, Lokshina I, Higashikubo R, Evans S, et al. Ferroptotic cell death and TLR4/Trif signaling initiate neutrophil recruitment after heart transplantation. J Clin Invest. 2019b;129(6):2293–304.

Núñez MT, Hidalgo C. Noxious iron-calcium connections in neurodegeneration. Front Neurosci. 2019;13(undefined):48.

Pujol-Giménez J, Hediger MA, Gyimesi G. A novel proton transfer mechanism in the SLC11 family of divalent metal ion transporters. Sci Rep. 2017;7(1):6194.

Simonis G, Mueller K, Schwarz P, Wiedemann S, Adler G, Strasser RH, et al. The iron-regulatory peptide hepcidin is upregulated in the ischemic and in the remote myocardium after myocardial infarction. Peptides. 2010;31(9):1786–90.

Xue X, Ramakrishnan S, Weisz K, Triner D, Xie L, Attili D, et al. Iron Uptake via DMT1 integrates cell cycle with JAK-STAT3 signaling to promote colorectal tumorigenesis. Cell Metab. 2016;24(3):447–61.

Yu H, Yang C, Jian L, Guo S, Chen R, Li K, et al. Sulfasalazine-induced ferroptosis in breast cancer cells is reduced by the inhibitory effect of estrogen receptor on the transferrin receptor. Oncol Rep. 2019;42(2):826–38.

Zhao H, Tao Z, Wang R, Liu P, Yan F, Li J, et al. MicroRNA-23a-3p attenuates oxidative stress injury in a mouse model of focal cerebral ischemia-reperfusion. Brain Res. 2014;1592(undefined):65–72.

Zhao Y, Sun X, Cao W, Ma J, Sun L, Qian H, et al. Exosomes derived from human umbilical cord mesenchymal stem cells relieve acute myocardial ischemic injury. Stem Cells Int. 2015;2015(undefined):761643.